# Enhancing industrial inspection with efficient edge illumination X-ray phase contrast simulations

# Enhancing industrial inspection with efficient edge illumination x-ray phase contrast simulations

Nicholas Francken
*dept. of physics (University of Antwerp)*
*imec-Vision Lab*
Antwerp, Belgium
nicholas.francken@uantwerpen.be

Pavel Paramonov
*dept. of physics (University of Antwerp)*
*imec-Vision Lab*
Antwerp, Belgium
pavel.paramonov@uantwerpen.be

Jan Sijbers
*dept. of physics (University of Antwerp)*
*imec-Vision Lab*
Antwerp, Belgium
jan.sijbers@uantwerpen.be

Jan De Beenhouwer
*dept. of physics (University of Antwerp)*
*imec-Vision Lab*
Antwerp, Belgium
jan.debeenhouwer@uantwerpen.be

***Abstract*—X-ray imaging is routinely used in non-destructive testing, where x-ray projections of an object are compared to a ground truth to detect anomalies. This ground truth can be simulated x-ray projections of a computer-aided design model of the object. While conventional x-ray imaging excels at distinguishing high from low absorbing materials, x-ray phase contrast imaging delivers higher contrast between different low absorbing materials. However, this requires efficient x-ray phase contrast imaging compatible computer-aided design projection simulation software, to generate the ground truth images. Currently available x-ray phase contrast imaging simulation tools are either notoriously slow Monte-Carlo simulators, or equally slow explicit wavefront propagation simulators. In this work, a recently developed computer-aided design projector toolbox is used to model the edge illumination x-ray phase contrast imaging setup within a GPU-based ray tracing framework, significantly speeding up simulations. Results for two industrial samples are shown. One has artificially introduced defects and the other is compared to a real edge illumination acquisition, demonstrating the potential to accurately and efficiently simulate phase contrast images, directly from a computer-aided design model. This paves the way for edge illumination to be applied in non-destructive testing.**

***Index Terms*—X-ray phase contrast imaging, edge illumination, computer simulation, inline inspection, non-destructive testing**

## I. Introduction

X-ray imaging is commonly used in non-destructive testing (NDT) to detect defects or other anomalies in objects [1]. A surface mesh of the object is compared to a ground truth, available in the form of a computer-aided design (CAD) model. The object surface mesh is extracted from a 3D reconstruction, which requires a large number of x-ray projections.

Industry 4.0 has shifted quality control expectations from scanning only representative samples to 100% inspection. The conventional, reconstruction-based, workflow is too slow to accommodate for this, and solutions, based for example on few-view 3D inspection, are being developed [2], [3].

Conventional x-ray imaging, however, few-view or otherwise, is based on x-ray attenuation, and provides contrast between high and low absorbing materials, while x-ray phase contrast imaging (XPCI) provides higher contrast between different so-called soft materials, which have a low x-ray absorption, but higher difference in refractive indices [4]. Moreover, differential XPCI setups, measuring the first derivative of the phase signal, show edge enhancement, and allow for easier detection of interfaces between materials. Additionally, many XPCI setups provide dark field contrast, which is related to the presence of unresolvable microstructures in a sample.

XPCI setups, however, typically have longer acquisition times, favoring projection-based methods in an NDT context. This requires efficient software that can generate phase contrast simulations of the ground truth CAD models. Popular simulation tools, such as the ASTRA toolbox [5], don't include phase effects, nor support simulations of CAD models. Current phase contrast and CAD model compatible solutions are limited to computationally expensive, and thus slow, explicit wavefront propagation [6] and Monte Carlo simulators [7].

Recently, a toolbox was developed to efficiently simulate x-ray radiographs of CAD models [8]. The toolbox includes ray tracing projection techniques, and supports x-ray refraction by applying Snell's law at the sample interfaces. Thus, so-called non-interferometric XPCI techniques, in which phase effects are described as x-ray refraction in a geometric optics framework, can be accurately modelled within this ray tracing simulation environment.

Edge illumination (EI) [9] is such a non-interferometric XPCI technique [10]. It employs two absorbing masks with slit-shaped apertures, one placed in front of the sample and one in front of the detector. The first mask splits the x-ray beam into smaller *beamlets*, and phase contrast is measured as beamlet refraction, while unresolvable microstructures, related to dark field, cause beamlet broadening.

In this work, the EI setup is modelled in a CAD-projector, demonstrating, to the best of our knowledge, for the first time, efficient and accurate EI-XPCI simulations, directly from a CAD model. Results for a PCB support with pore defects are shown and those for a fuse cover are favorably compared with

a real EI acquisition. This paves the way for NDT applications, such as fast inline inspection, including phase contrast.

## II. Theory & Methods

### A. Edge Illumination

In a conventional x-ray setup, a sample is placed between an x-ray source and a detector. X-rays going through the sample are attenuated, providing contrast in the projections. The EI setup is constructed by adding two absorbing masks to the imaging setup, one in front of the sample and the other in front of the detector, as illustrated in Fig. 1. Both these masks have slit shaped apertures, typically with a period equal to (a multiple of) the (demagnified) detector pixel size. The sample mask splits the x-ray beam into smaller *beamlets*, while the detector mask covers the edges of the detector pixel columns (or rows), creating insensitive regions on the detector. Usually, the detector mask remains fixed, while the sample mask is stepped perpendicular to the mask apertures during the acquisition.

This stepping, referred to as phase stepping, generates an intensity modulation on the detector pixels, which can be plotted in function of the sample mask displacement (relative to perfect alignment), resulting in the so-called illumination curve (IC). The IC can be measured both with (sample IC) and without (flatfield IC) a sample present. Assuming the IC can be approximated by a Gaussian fit, three different contrasts (attenuation, phase and dark field) can be retrieved from the fitting parameters [11].

The attenuation signal is related to the change in area under the IC, while the phase contrast is related to the shift of the mean IC position, and the dark field to the IC broadening. Whereas the phase image gives a higher contrast version of the attenuation, the dark field provides new and complementary information.

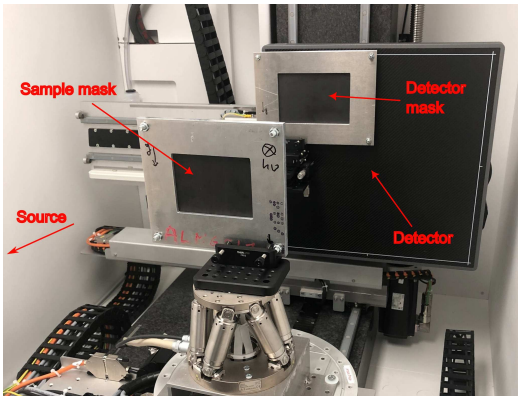


Fig. 1. The edge illumination setup.

### B. Simulation framework

The refraction enabled ray tracing projector in a recently developed toolbox was used [8]. The highly parallel nature of ray tracing is leveraged by using the NVIDIA OptiX ray tracing engine to provide performant, GPU-accelerated simulations. The projector supports triangular surface meshes as input. Each mesh is given a linear attenuation coefficient and refractive index as material properties. The former is used, together with the ray path length through each mesh, in the Beer-Lambert law to determine the ray attenuation, while the latter is applied in Snell's law to change the ray direction at the mesh interfaces between two materials.

The above method, because of the energy dependence of the material properties, generates monochromatic projections for a certain x-ray energy. For this work, the toolbox was extended to include polychromatic simulations by summing weighted monochromatic projections, where the weights are determined by the specifics of the imaging setup that is being modelled (e.g., the source spectrum and/or the detector response).

To model the EI setup, the two absorbing masks are introduced as surface meshes, and the EI acquisition scheme was implemented by applying mesh translation transformations to the sample mask mesh for the different phase steps.

Furthermore, the number of rays that are cast per detector pixel can be controlled. This is necessary to accurately model the EI setup, as a single, infinitesimally thin ray per pixel (which is the default) cannot adequately model the refraction of a finite width beamlet. To compensate for this, the number of rays that are cast in the phase-sensitive direction (i.e., perpendicular to the mask apertures) was increased until the finite width of the beam was adequately modeled.

## III. Experiments

The EI setup that was modeled in this work, mimicked the one in our FleXCT system [12], [13]. The source to detector distance (SDD) was $1.8\,\mathrm{m}$, while the source to object distance (SOD) was $1.2\,\mathrm{m}$. The sample and detector mask were placed $5\,\mathrm{cm}$ in front of the sample and detector, respectively. The detector pixel size was $150\,\mu\mathrm{m} \times 150\,\mu\mathrm{m}$ and the projected aperture width of the masks was $30\,\mu\mathrm{m}$ (at the detector plane), while the aperture period matched the demagnified pixel width. The masks were $225\,\mu\mathrm{m}$ thick and made out of gold. The sample mask was moved along 11 equally spaced phase steps in the $[-40\,\mu\mathrm{m},\ 40\,\mu\mathrm{m}]$ interval, relative to perfect alignment with the detector mask. For the CAD-projector, 2000 rays were cast per detector pixel, to properly model the beamlets generated by the sample mask, and Poisson noise was added to the projections, after scaling them to the same intensity range as the FleXCT scans.

As a first experiment, a PCB support CAD model was modified to include pore-like defects (see Fig. 2) and radiographs were simulated using a modeled version of the FleXCT system EI setup in the CAD-projector. For this simulation, the dithering technique was applied, where the sample was shifted multiple times, at sub-pixel distances, laterally to the mask apertures, to increase the radiograph resolution along the lateral direction. Five equally spaced dither steps in the $[-45\,\mu\mathrm{m},\ 45\,\mu\mathrm{m}]$ interval were simulated, and the resulting projections were stitched together into a single high-resolution image. As comparison, a conventional radiograph was simulated, without the EI masks presents, where the SOD was

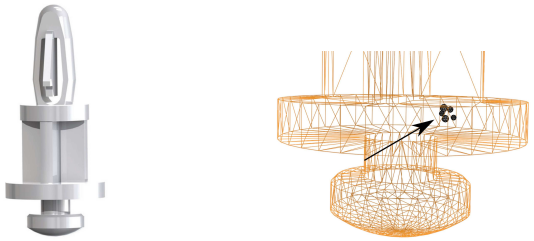

(a) Render (b) Pore defects

Fig. 2. The PCB support sample: (a) shows a render of the CAD model and (b) shows the internal pore-like defects.

(a) Photograph (b) Render

Fig. 3. The fuse cover sample: (a) shows a photograph of the real sample and (b) shows a render of the CAD model.

decreased to 24 cm, keeping the SDD constant, accounting for the higher resolution in the dithered EI simulation. The material properties for the PCB support sample were set to those of nylon 66. Linear attenuation coefficients and refractive indices at different energies were used in the CAD-projector to simulate polychromatic projections for a source set at 65 kVp. A source spectrum and detector scintillator response were estimated using Monte Carlo simulations and given in Fig. 4. The weights for the weighted sum of the different monochromatic projections were determined by multiplying both energy-dependent profiles. Because there were no microstructures in the sample, this experiments looks only at the attenuation and phase contrasts.

As a second experiment, an industrial fuse cover sample (see Fig. 3) was scanned using the EI setup in the FleXCT system, and radiographs of its CAD model were simulated using the CAD-projector. The three contrasts from a single radiograph, without dithering, were considered. The source was set to 65 kVp and 40 W, while every phase step of the sample mask had an exposure time of 1.5 s and 3 averages were acquired. A region of interest containing the sample of 300 by 150 pixels was selected. The fuse cover sample consists of 25% glass fiber reinforced nylon 66, but due to the lack of available information on that exact material composition, the material properties for standard nylon 66 were used. Linear attenuation coefficients, refractive indices, and the projection weights at different energies were set identical to the PCB support experiment.

## IV. Results & Discussion

The conventional attenuation and EI phase contrast of the simulated PCB support with pore defects is shown in

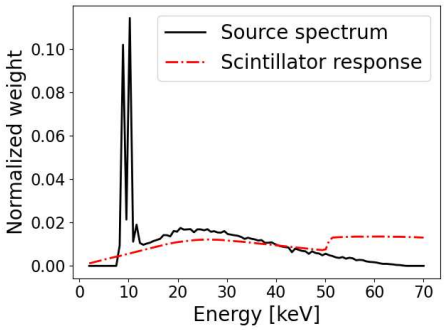


Fig. 4. Estimated normalized weights for the FleXCT spectrum and scintillator response, based on Monte Carlo simulations.

Fig. 5. The attenuation image (Fig. 5a), which used a higher magnification, has a resolution of 20 µm, while the phase contrast image (Fig. 5b), because of the dithering process, has a vertical resolution of 100 µm and horizontal resolution of 20 µm. Fig. 5a and 5b also show an inset zoom on the pores and line profiles (Fig. 5c) going through two of the pores. The phase contrast image shows, as expected, a higher contrast for the pores than the conventional attenuation image.

Note that, in projection space, the EI setup does not measure the x-ray phase shift directly, but rather the ray refraction, which is related to the first derivative of the phase shift, resulting in edge enhancement in what colloquially is being referred to here as the phase contrast.

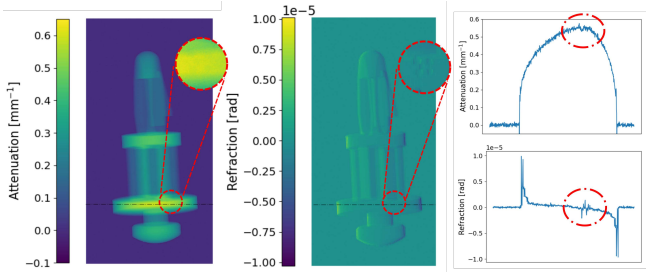


(a) Attenuation (b) Refraction (c) Line profiles

Fig. 5. The conventional attenuation contrast (a), EI phase contrast (b) and line profiles for the dashed lines (c) of attenuation (top) and refraction (bottom) for the PCB support with pore defects CAD model simulation.

A single projection of the simulation took on average 1.8 s and was looped over the different phase steps, dithering steps and source spectrum sample points.

For the fuse cover sample, the attenuation, phase and dark field contrasts of the FleXCT data are shown in Fig. 6, while the CAD-projector simulation results are shown in Fig. 7.

For now, the pose of the CAD model was set manually to closely match that of the real sample. In the future, we will apply a pose estimation technique such as in [2], which could in turn be upgraded by including the extra contrasts provided in EI acquisitions.

The attenuation contrast shows, on average, a higher attenuation for the FleXCT projection. This is likely caused by the

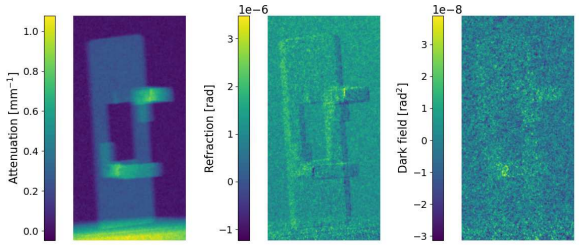


Fig. 6. From left to right, the attenuation, phase, and dark field contrasts for the fuse cover sample EI scan in the FleXCT system.

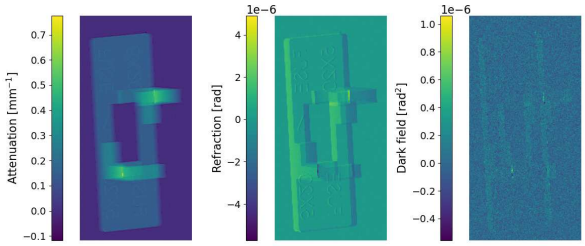


Fig. 7. From left to right, the attenuation, phase, and dark field contrasts for the fuse cover CAD model EI simulations in the CAD-projector.

estimated linear attenuation coefficient in the EI simulations, for which nylon 66 was used, not taking into account the 25% of glass fibers in the composite, and by the simplified detector model.

The phase (i.e., refraction) contrast has more sharply defined edges, and a similar magnitude of values between the real and simulated data is observed. The simulated signal is slightly stronger, which is likely caused by the idealized smooth surfaces and sharp edges in the CAD model. Methods exist to compensate for this, by artificially introducing a so-called surface roughness [14].

In the dark field contrast, the simulated signal shows the outline of the fuse cover sample. The real projection, however, shows a bright spot on the lower left side. A separate, conventional x-ray computed tomography (CT) scan was performed, and a 3D reconstruction was generated (see Fig. 8). In the reconstruction, an internal defect can be spotted at the same location of the dark field signal bright spot in the EI projection (the dashed red circle in Fig. 8). This indicates the potential of the dark field contrast to detect small sample defects, such as (micro)cracks or pores, which are more difficult to see in the other contrasts.

In general, the contrasts of the fuse cover show qualitatively similar profiles, and the differences, for example in the dark field signal, can be used to detect defects. For quantitative results, improvements should be made to the sample pose and material property estimations, and a more refined detector model should be used.

Furthermore, the efficiency of the simulations can be improved further by moving the loops over the different projections completely to the GPU, removing a substantial CPU to GPU data transfer overhead.

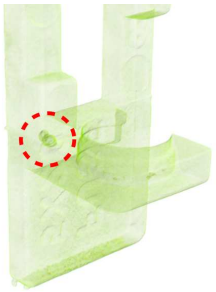

Fig. 8. Render of a 3D reconstruction of the fuse cover sample from a conventional CT scan, with the internal defect marked in the dashed circle.

To conclude, it is important to mention some radiation dose considerations, as, even though they are less prevalent in industrial settings, they are still an important part of x-ray imaging. The presented edge illumination setup requires multiple projections of the sample (at minimum three) to enable phase retrieval and extract the different contrasts. The hence incurred increase in radiation time, however, is offset by the inclusion of the sample mask, which blocks most of the x-ray beam (typically around 80 % for fully absorbing masks) before it reaches the sample.

## V. Conclusion

The edge illuminated phase contrast setup was modeled for the first time in an efficient GPU-accelerated ray tracing toolbox. The toolbox allows simulating x-ray projections directly from a CAD model, making it ideally suited for NDT, while the addition of edge illumination allows for the exploration of using phase contrast setups in NDT applications such as inline inspection.

## Acknowledgment

This research is funded by the Research Foundation Flanders (FWO) projects G094320N, G090020N, and FoodPhase (S003421N).

## References

[1] L. De Chiffre, S. Carmignato, J.-P. Kruth, R. Schmitt, and A. Weckenmann, "Industrial applications of computed tomography," *CIRP Annals*, vol. 63, no. 2, pp. 655–677, 2014.

[2] A. Presenti, J. Sijbers, and J. De Beenhouwer, "Dynamic few-view x-ray imaging for inspection of cad-based objects," *Expert Systems with Applications*, vol. 180, p. 115012, 2021.

[3] A. Presenti, Z. Liang, L. Pereira, J. Sijbers, and J. De Beenhouwer, "Fast and accurate pose estimation of additive manufactured objects from few x-ray projections," *Expert Systems with Applications*, vol. 213, p. 118866, 09 2022.

[4] M. Endrizzi, "X-ray phase-contrast imaging," *Nuclear Instruments and Methods in Physics Research Section A: Accelerators, Spectrometers, Detectors and Associated Equipment*, vol. 878, pp. 88–98, 2018, radiation Imaging Techniques and Applications.

[5] W. van Aarle *et al.*, "Fast and flexible X-ray tomography using the ASTRA toolbox," *Opt. Express*, vol. 24, no. 22, pp. 25 129–25 147, Oct 2016.

[6] T. Faragó *et al.*, "Syris: A flexible and efficient framework for X-ray imaging experiments simulation," *Journal of Synchrotron Radiation*, vol. 24, no. 6, pp. 1283 – 1295, 2017.

[7] J. Sanctorum, J. D. Beenhouwer, and J. Sijbers, "X-ray phase contrast simulation for grating-based interferometry using GATE," *Opt. Express*, vol. 28, no. 22, pp. 33 390–33 412, Oct 2020.

[8] P. Paramonov, J. Renders, T. Elberfeld, J. D. Beenhouwer, and J. Sijbers, "Efficient X-ray projection of triangular meshes based on ray tracing and rasterization," in *Proc. SPIE 12242*, 2022, p. 122420W.
[9] A. Olivo, "Edge-illumination X-ray phase-contrast imaging," *Journal of Physics: Condensed Matter*, vol. 33, no. 36, p. 363002, 2021.
[10] P. R. Munro, K. Ignatyev, R. D. Speller, and A. Olivo, "The relationship between wave and geometrical optics models of coded aperture type x-ray phase contrast imaging systems," *Opt. Express*, vol. 18, no. 5, pp. 4103–4117, Mar 2010.
[11] M. Endrizzi and A. Olivo, "Absorption, refraction and scattering retrieval with an edge-illumination-based imaging setup," *Journal of Physics D: Applied Physics*, vol. 47, no. 50, p. 505102, nov 2014.
[12] B. De Samber *et al.*, "FleXCT: a flexible X-ray CT scanner with 10 degrees of freedom," *Opt. Express*, vol. 29, no. 3, pp. 3438–3457, 2021.
[13] J. Sanctorum, N. Six, J. Sijbers, and J. D. Beenhouwer, "Augmenting a conventional x-ray scanner with edge illumination-based phase contrast imaging: how to design the gratings," in *Proc. SPIE 12242*, 2022, p. 1224218.
[14] J. Sanctorum, J. Sijbers, and J. De Beenhouwer, "Dark Field Sensitivity In Single Mask Edge Illumination Lung Imaging," in *2021 IEEE 18th International Symposium on Biomedical Imaging (ISBI)*, 2021, pp. 775–778.